The 2011 Magnitude 9.0 Tohoku-Oki Earthquake: Mosaicking the Megathrust from Seconds to Centuries

Mark Simons, *et al.*

Science **332**, 1421 (2011);
DOI: 10.1126/science.1206731

similar to those of a simple shear fault propagating along the seismogenic zone. The rise time at both stations is close to 20 s, so that we can approximate the width of the fault as twice (because of upward and downward propagation) the product of this time multiplied by the rupture speed. We obtain a fault width of ~120 km, which is in agreement with our static modeling. Some motograms (especially SJAV) also reveal an arrival (or "kink") that may be due to a possible rupture velocity variation as rupture reaches the northern asperity (fig. S4). We attribute this arrival to the triggering of rupture in the northern asperity (the largest one), ~60 s after the initiation of the rupture. This arrival would mark the instant when the Maule event became a megathrust earthquake.

Comparing the 2010 Maule megathrust earthquake rupture with earlier events is important for seismic hazard assessment, but the lack of precise information about some past events requires caution. The 2010 rupture broke well beyond the previously identified gap left by the 1835 earthquake, which appears to have had a shorter rupture length of about 350 km and a smaller magnitude. The shorter rupture of 1835 corresponds roughly to the length attained by the 2010 rupture at the critical instant captured at 60 s in the motograms. This is before rupture of the main northern asperity, which may have reached the trench, thus contributing strongly to generation of the tsunami that struck the coast of Constitución (~5 m of minimum inundation over a large latitudinal extent). The absence of large tsunami at Constitución in 1835 (*4*) is consistent with lack of rupture of the northern asperity during that event. The 2010 rupture covered the M_w 7.6 Talca earthquake of 1928, which may have been an event located near the transition zone similar to the 2007 M_w 7.7 Tocopilla earthquake (*7*, *23*) in Northern Chile. The ~500-km-long 2010 rupture overlaps laterally (over ~100 km) also with the ruptures of three earthquakes that occurred earlier on its southern and northern edges: to the south, the 21 May 1960 Concepcion event (M_w 8.3) and the Valdivia earthquake of 22 May 1960 (M_w 9.5); to the north, the rupture zone of the 1906 M_w 8.5 Valparaíso earthquake. This suggests interleaved tapering of coseismic slip in those overlapping regions, probably involving, over the long term, accommodation of deformation by both seismic and aseismic processes.

References and Notes

1. R. Bilham, *Science* **308**, 1126 (2005).
2. C. Vigny *et al.*, *Nature* **436**, 201 (2005).
3. C. Darwin, *Journal of Researches into the Natural History and Geology of the Countries Visited During the Voyage of the H.M.S. Beagle Round the World* (John Murray, London, 1876).
4. R. FitzRoy, *Narrative of the Surveying Voyages of His Majesty's Ships Adventure and Beagle Between the years 1826 and 1836, Describing Their Examination of the Southern Shores of South America, and the Beagle's Circumnavigation of the Globe* (Henry Colburn, London, 1839).
5. F. Montessus de Ballore, *Historia Sismica de los Andes Meridionales, 6 vols.* (Editorial Cervantes, Santiago de Chile, 1916).
6. C. Lomnitz, *Geofis. Panamericana* **1**, 151 (1971).
7. S. L. Beck, S. Barrientos, E. Kausel, M. Reyes, *J. S. Am. Earth Sci.* **11**, 115 (1998).
8. R. Madariaga, M. Métois, C. Vigny, J. Campos, *Science* **328**, 181 (2010).
9. S. Nishenko, *J. Geophys. Res.* **90**, 3589 (1985).
10. Z. Altamimi, X. Collilieux, J. Legrand, B. Garayt, C. Boucher, *J. Geophys. Res.* **112**, B09401 (2007).
11. J. Campos *et al.*, *Phys. Earth Planet. Inter.* **132**, 177 (2002).
12. J. C. Ruegg *et al.*, *Geophys. Res. Lett.* **29**, 1517 (2002).
13. J. C. Ruegg *et al.*, *Phys. Earth Planet. Inter.* **175**, 78 (2009).
14. Materials and methods are available as supporting material on *Science* Online.
15. M. Farías *et al.*, *Science* **329**, 916 (2010).
16. X. Tong *et al.*, *Geophys. Res. Lett.* **37**, L24311 (2010).
17. M. Moreno, M. Rosenau, O. Oncken, *Nature* **467**, 198 (2010).
18. T. Lay *et al.*, *Geophys. Res. Lett.* **37**, L13301 (2010).
19. B. Delouis, J.-M. Nocquet, M. Vallée, *Geophys. Res. Lett.* **37**, L17305 (2010).
20. S. Lorito *et al.*, *Nat. Geosci.* **4**, 173 (2011).
21. R. D. Hyndman, M. Yamano, D. A. Oleskevich, *Isl. Arc* **6**, 244 (1997).
22. T. Tanimoto, C. Ji, *Geophys. Res. Lett.* **37**, L22312 (2010).
23. M. Béjar-Pizarro, D. Carrizo, A. Socquet, R. Armijo, and the North Chile Geodetic Team, *Geophys. J. Int.* (2010).

Acknowledgments: We thank the International GNSS Service; Instituto Geográfico Nacional, Argentina; Instituto Brasileiro de Geografia e Estatística, Brasil; and Transportable Integrated Geodetic Observatory/ Bundesamt für Kartographie und Geodäsie Frankfurt/ Universidad de Concepcion for access to their cGPS data in South America. We are also thankful to the French Institut National des Sciences de l'Univers, the Institut pour la Recherche et le Développment, the Agence Nationale pour la Recherche, and the Ministère des Affaires Etrangères for providing financial support. We also thank members of the Laboratoire International Associé Montessus de Ballore and the many individuals who participated in field campaigns and network maintenance over the years. This is IPGP contribution #3161.

Supporting Online Material

www.sciencemag.org/cgi/content/full/science.1204132/DC1
Materials and Methods
SOM Text
Figs. S1 to S14
Tables S1 to S4
References (*24*–*35*)

10 February 2011; accepted 20 April 2011
Published online 28 April 2011;
10.1126/science.1204132

The 2011 Magnitude 9.0 Tohoku-Oki Earthquake: Mosaicking the Megathrust from Seconds to Centuries

Mark Simons,[1]* Sarah E. Minson,[1] Anthony Sladen,[1,2] Francisco Ortega,[1] Junle Jiang,[1] Susan E. Owen,[3] Lingsen Meng,[1] Jean-Paul Ampuero,[1] Shengji Wei,[1] Risheng Chu,[1] Donald V. Helmberger,[1] Hiroo Kanamori,[1] Eric Hetland,[4] Angelyn W. Moore,[3] Frank H. Webb[3]

Geophysical observations from the 2011 moment magnitude (M_w) 9.0 Tohoku-Oki, Japan earthquake allow exploration of a rare large event along a subduction megathrust. Models for this event indicate that the distribution of coseismic fault slip exceeded 50 meters in places. Sources of high-frequency seismic waves delineate the edges of the deepest portions of coseismic slip and do not simply correlate with the locations of peak slip. Relative to the M_w 8.8 2010 Maule, Chile earthquake, the Tohoku-Oki earthquake was deficient in high-frequency seismic radiation—a difference that we attribute to its relatively shallow depth. Estimates of total fault slip and surface secular strain accumulation on millennial time scales suggest the need to consider the potential for a future large earthquake just south of this event.

The 2011 Tohoku-Oki earthquake occurred on the megathrust where the Pacific Plate subducts below Japan at an average rate of about 8 to 8.5 cm/year (Fig. 1) (*1*). Historically, many moment magnitude (M_w) 7 to M_w 8 earthquakes have occurred on the Japan Trench megathrust (*2*). Geodetic observations of crustal strain during the interseismic period have been used to infer spatial variations in the degree of plate coupling (i.e., regions of the megathrust expected to produce large earthquakes) for this section of the Japan Trench (*3*). Generally, these models infer high coupling in regions where earthquakes were known to have already occurred (Fig. 1 and fig. S1), with only partial or even no coupling from the trench to a point approximately midway between the trench and the coastline—precisely the region where the 2011 Tohoku-Oki earthquake occurred. It is fundamentally difficult to use land-based data to assess the state of coupling on distant portions of a megathrust. The Jogan earthquake of 13 July 869 may be the only documented event to have occurred with a possible magnitude and location similar to that of the 2011 earthquake (*4*).

Observations of the 2011 Tohoku-Oki earthquake from a dense regional geodetic network

[1]Seismological Laboratory, Division of Geological and Planetary Sciences, California Institute of Technology, Pasadena, CA 91125, USA. [2]Geoazur, Observatoire de la Côte d'Azur, Université de Nice–Sophia Antipolis, CNRS, IRD, Valbonne, 06103 Nice Cedex 2, France. [3]Jet Propulsion Laboratory, California Institute of Technology, Pasadena, CA 91109, USA. [4]Department of Geological Sciences, University of Michigan, Ann Arbor, MI 48109, USA.

*To whom correspondence should be addressed. E-mail: simons@caltech.edu

and globally distributed broadband seismographic networks, as well as open-ocean tsunami data, allow the construction of a family of models that describe the distribution and evolution of subsurface fault slip. Surface displacements due to the Tohoku-Oki earthquake were observed by more than 1200 continuously recording Global Positioning System (GPS) sites installed and operated by the Geodetic Survey of Japan (GSI). Here, we used data sampled at 5-min intervals to produce individual three-component positional time series, from which we isolated coseismic displacements (Fig. 1) (*5*). Significant quasi-permanent displacements due to the mainshock occurred over the entire northern half of Honshu, with peak GPS-measured offsets exceeding 4.3 m horizontally and 66 cm of subsidence (Figs. 1 and 2). We also isolated surface displacements associated with an M_w 7.9 aftershock that occurred about 30 min after the mainshock (Fig. 1). The spatial extent and the azimuth of the horizontal displacement vectors indicate that the aftershock was located to the south of the mainshock in the Ibaraki segment. Peak horizontal GPS-measured displacements for this aftershock were approximately 44 cm (Fig. 1). We used observations of open-ocean tsunami wave heights measured by deep sea-bottom pressure gauges to constrain the distribution of coseismic slip on the shallowest portions of the megathrust (Fig. 1). On the basis of their spatial and azimuthal distribution, we selected 12 sensors in the Pacific ocean east of the Japan trench. The closest of these pressure gauges detected a maximum tsunami wave height of more than 1.9 m (Fig. 2A).

We first describe static coseismic slip models based on the GPS observations of coseismic offsets and the sea-floor pressure gauge data (Fig. 3 and fig. S2). Static models constrain the final distribution of slip for the event but not its temporal evolution. We adopt a novel fully Bayesian probabilistic formalism requiring no a priori spatial regularization (*5*, *6*). We conservatively define the section of the megathrust directly involved with the earthquake by considering only the areas where inferred slip exceeds 8 m (approximately 15% of the maximum slip value, depending on the model). The model predicts maximum seafloor subsidence of about 2 m located 50 km offshore Sendai and Kamaishi, and maximum seafloor uplift just under 9 m about 50 km from the trench (Fig. 2). This model fits the GPS and tsunami data with variance reductions of 99.7% and 90.1%, respectively. Residual GPS displacements after removal of the model predictions are shown in fig. S3.

The spatial distribution of slip (Fig. 3) can be divided into several sections. The central section contains the highest estimated slip values, with peak displacement of around 60 m. The up-dip limit of the forearc is an active accretionary prism that extends about 50 km landward of the trench. Generally, the majority of the fault slip does not extend below this zone, with the exception being just up-dip of the region of maximum fault slip where estimated slip values near the trench range from about 5 to 15 m. A tendril of slip extends more than 100 km north from the central slip zone and just down-dip from the inferred source of the 1896 M_w 8.0 Sanriku earthquake. Average slips in this region are approximately 5 to 10 m—similar to those inferred for the 1896 earthquake (*7*). A lobe of about 10 m of fault slip extends down-dip toward the Oshika Peninsula east-northeast of Sendai. This lobe overlaps several of the inferred historical Miyagi-Oki rupture areas. Slip in the up-dip portion of these rupture areas exceeds 20 m. Another tendril of significant slip (5 to 10 m) extends southward of the main high-slip asperity. This tendril clearly overlaps the inferred locations of the 1938 Fukushima earthquake sequence.

We estimated probability distributions for derived scalar rupture quantities including rupture area, potency, scalar seismic moment, and static stress drop (fig. S4). Estimates of moment magnitude range from 8.8 to 9.2. We note that static slip models are relatively insensitive to absolute scaling of the elastic moduli; thus, estimates of moment are less certain than estimates of potency. Estimates of static stress drop vary between 2 and 10 MPa, depending on the area of fault considered. These values are high relative to previous estimates for megathrust events, which typically lie in the 1 to 5 MPa range (*8*) and reflect the relatively small area over which there is high slip. As a point of comparison, relative to our model for the Tohoku-Oki event, models of the 2010 M_w 8.8 Maule, Chile earthquake typically find twice the along-strike extent of slip and half the peak slip (*9*, *10*).

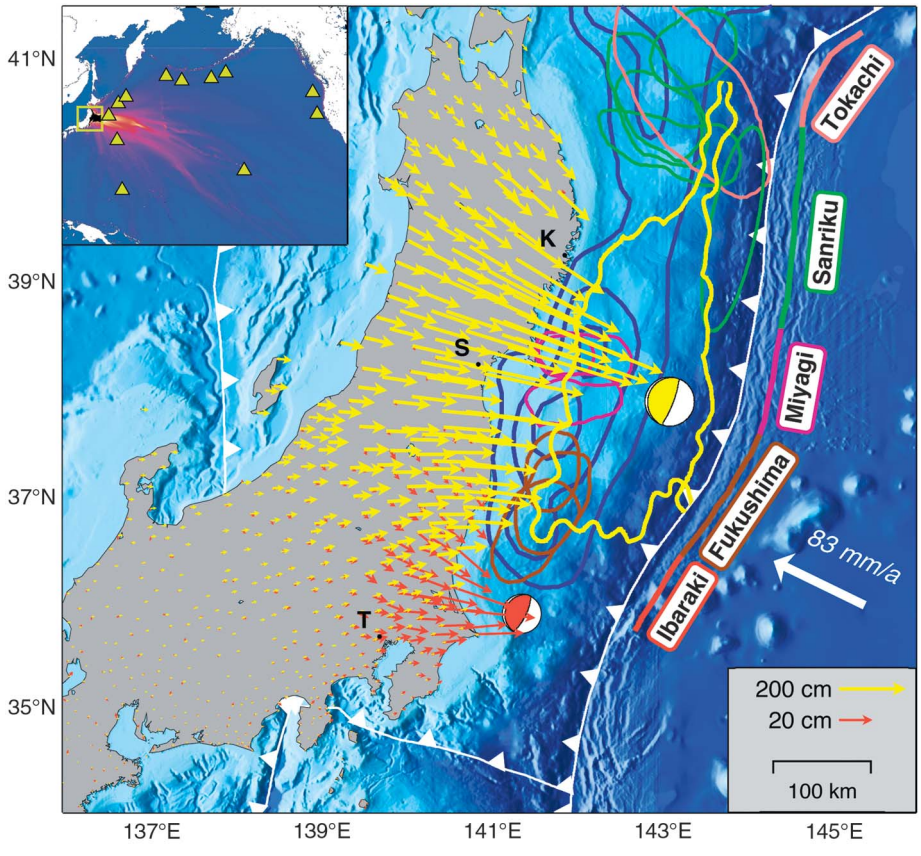

Fig. 1. Map of central and northern Honshu, Japan. Vectors indicate the horizontal component of the GPS displacements for the mainshock (yellow) and the M_w 7.9 aftershock (orange). Approximate locations of historical megathrust earthquakes are indicated by closed curves colored by region: pink, Tokachi (1968 *M*8.2); green, Sanriku (1896 *M*8.5, 1901 *M*7.4, 1931 *M*7.6, 1933 *M*7.6); purple, Miyagi (1897 *M*7.4, 1936 *M*7.4, 1978 *M*7.4, 2005 *M*7.2); brown, Fukushima (1938 M_w 7.4, 1938 M_w 7.7, 1938 M_w 7.8) [modified from (*2*, *3*, *33*)]. Yellow and orange moment tensors indicate the W-phase centroid for the mainshock (*34*) and the GCMT (global centroid moment tensor) location for the *M*7.9 aftershock. The closed yellow curve indicates the outline of the M_w 9.0 mainshock (8 m slip contour). The region of inferred slip deficit or high plate coupling is indicated by dark blue nested contour lines for 35%, 70%, and 100% coupling (*3*). Barbed lines indicate subduction plate boundaries. The white arrow indicates the direction of convergence between the Pacific Plate and northeast Japan (*1*). T, S, and K indicate the cities of Tokyo, Sendai, and Kamaishi. The yellow box in the inset reference map shows the region of this figure and the locations of deep-sea bottom pressure gauges used in this study, all superimposed on the peak tsunami wave heights predicted by our preferred earthquake source model.

We also developed two kinematic finite fault models based on one and two fault planes, respectively, and constrained by broadband seismic data and GPS observations (but no tsunami data) (*5*, *11*). Examples of the displacement and velocity waveform fits are shown in fig. S5. The inferred moment rate function suggests that most of the rupture occurred in a little over 3 min (fig. S6). We find a low average rupture velocity of about 1.2 km/s (fig. S6). This model explains 99% of the variance of the GPS data. The peak estimated fault slip in this model is about 45 m, a little less than found in the static model. This difference is due to the imposed smoothing in the kinematic model, which is absent in the static model. The extension of slip to the south (offshore Fukushima) is evident in the kinematic model; however, it is located up-dip relative to the static model, presumably because of the absence of the tsunami constraints in the kinematic model. The M_w 7.9 aftershock occurred just beyond the southernmost extent of the mainshock slip area with an estimated maximum slip of about 4 m for this event (Fig. 3) (*5*).

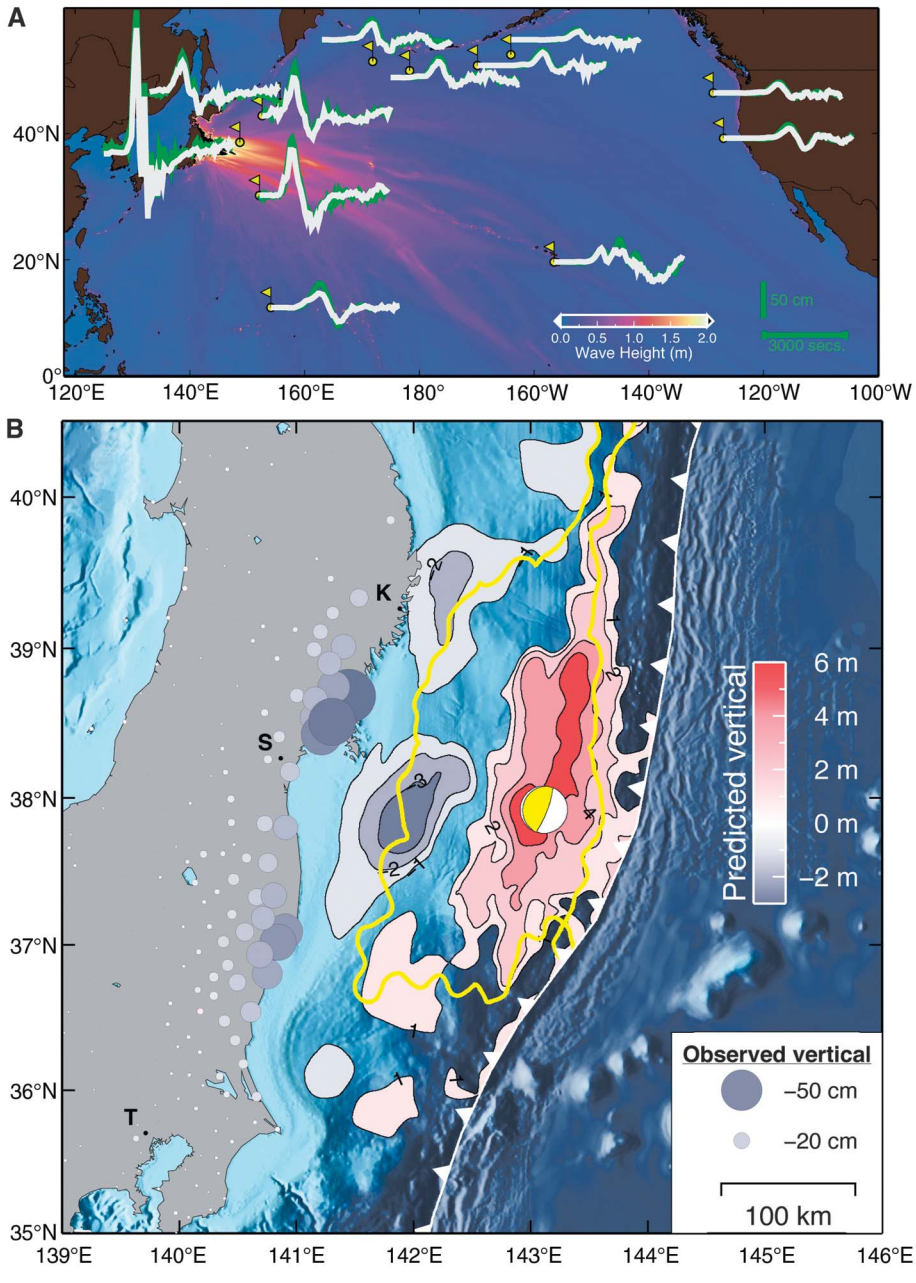

Fig. 2. (**A**) Observed (green) and predicted (white) deep ocean tsunami records of the Tohoku-Oki earthquake. The predicted records correspond to a model constructed using the mean of each fault slip parameter in the Bayesian inversion. These waveforms are superimposed on the map of maximum model-predicted tsunami height. (**B**) GPS vertical coseismic surface displacements (circles colored and scaled with amplitude) as well as model-predicted vertical sea-floor displacements (filled contours). Other overlay features are as in Fig. 1.

Observations at the high-frequency (HF) end of the seismic spectrum (2 to 4 Hz) can constrain rupture direction and duration (*12*); 90% of the energy release in this frequency band occurs within about 3 min (fig. S7). Unilateral rupture propagation would result in an azimuthally dependent duration. This earthquake displays uniform durations at most azimuths with slightly shortened durations in the down-dip direction, suggesting bilateral along-strike rupture with some down-dip propagation (fig. S7).

We developed an image of the rupture process at high frequencies (between 0.5 and 1 Hz) using back-projection of teleseismic array waveforms (*13*) based on high-resolution array processing techniques (*5*, *14*, *15*). The most energetic of the HF sources as a function of time during the rupture are systematically down-dip of the regions of largest fault slip (Fig. 3). The robustness of the locations of the HF radiators relative to the assumed hypocenter is supported by the consistency between the results obtained with USArray data and those from the European array (Fig. 3 and fig. S8).

HF radiation is usually assumed to be spatially correlated to seismic slip (*16*) or uniformly distributed over the fault (*17*). This assumption contrasts with the spatial complementarity between HF and low-frequency (LF) source properties observed for this earthquake. Such a relationship has been inferred for other earthquakes, although not systematically (*18*), and might reflect the general lack of correlation between HF and LF in ground motions (*19*, *20*). Dynamic rupture models generate HF radiation mostly during sudden changes of rupture speed along sharp contrasts of fault rheology or geometry, or along remnant stress concentrations from previous earthquakes (*21*), which can define the boundaries of the slip area.

Instead of relying on characteristics of the rupture dynamics to explain the predominance of HF radiators down-dip of the region of significant coseismic slip, an alternative explanation is that they occur at the transition between brittle and ductile regions. Recent observations of medium-sized earthquakes down-dip from aseismic sections as well as of slow-slip and nonvolcanic tremor phenomena suggest the presence of frictional heterogeneities in the brittle-ductile transition regions of subduction megathrusts (*22*). Coseismic triggering of compact brittle asperities embedded in the ductile fault matrix could explain the relative locations of HF and lower-frequency slip and the apparent lack of HF radiators at shallow depths.

Similarly, we find that large aftershocks with thrust mechanisms are located outside the region of coseismic slip (fig. S2), as has been documented for previous events (*23*, *24*). Interestingly, for this event, aftershocks are dominantly down-dip of the regions of major coseismic slip—consistent with the idea that fault slip at shallow depths is relatively slow because of higher fracture energy and thus radiates energy less efficiently than at greater depths (*8*). This latter interpretation is supported by a comparison of seismic excitation

Fig. 3. Inferred distribution of subsurface fault slip (color and black contours with a contour interval of 8 m). Fault slip associated with the M_w 7.9 aftershock is indicated by nested 1-m orange contours. Historic earthquake ellipses are as in Fig. 1. Location of points of HF radiation estimated using back-projection methods with data from the European Union seismic array and the USArray are indicated by squares and circles, respectively, with color intensity indicating time of the activity relative to the beginning of the event and with symbol size proportional to amplitude of the HF radiation normalized to the peak value. The star indicates the location of the Japan Meteorological Agency epicenter. See fig. S2 for a plot of the slip model without overlays.

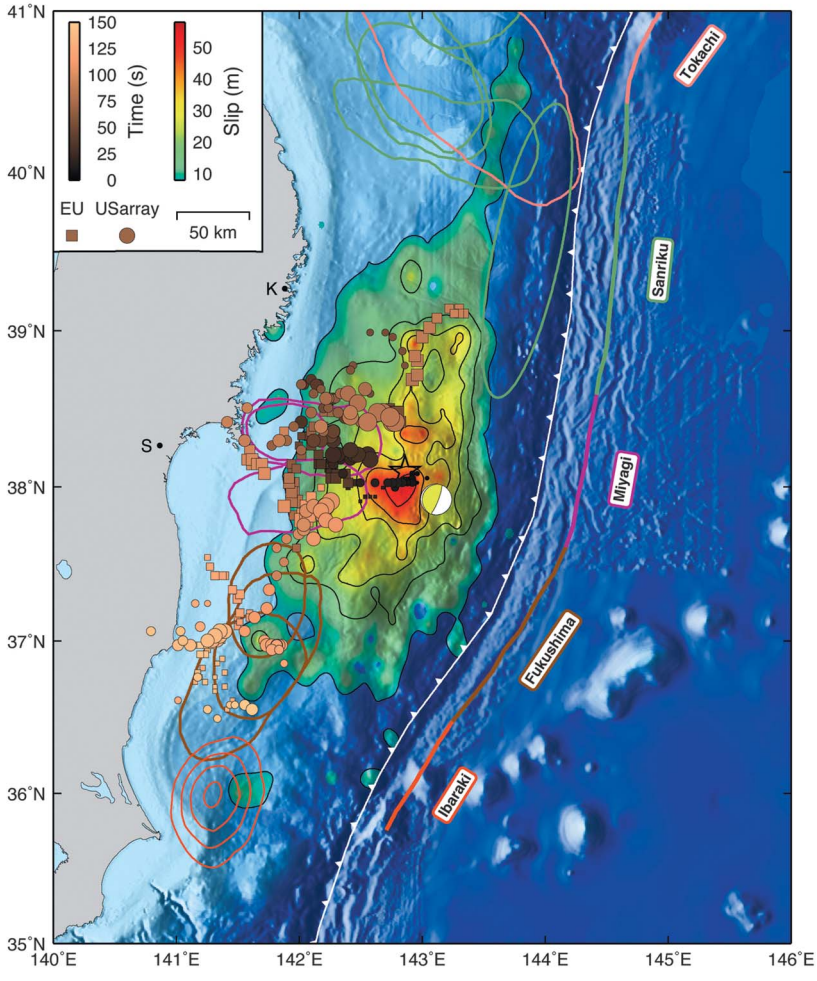

Fig. 4. Secular interseismic surface deformation (blue vectors) as observed by the GEONET continuous GPS network using the GSI F2 solution. The upper left inset shows the decrease of this deformation field at the latitude of the Miyagi (purple profile) and Ibaraki (orange profile) segments, with distance measured along the profile. The coseismic slip distribution is indicated by the yellow contours at 8-m intervals. The inset uses vectors within 100 km of the profile location. The question mark indicates a region of possible high seismic hazard. Other features are as in Fig. 1.

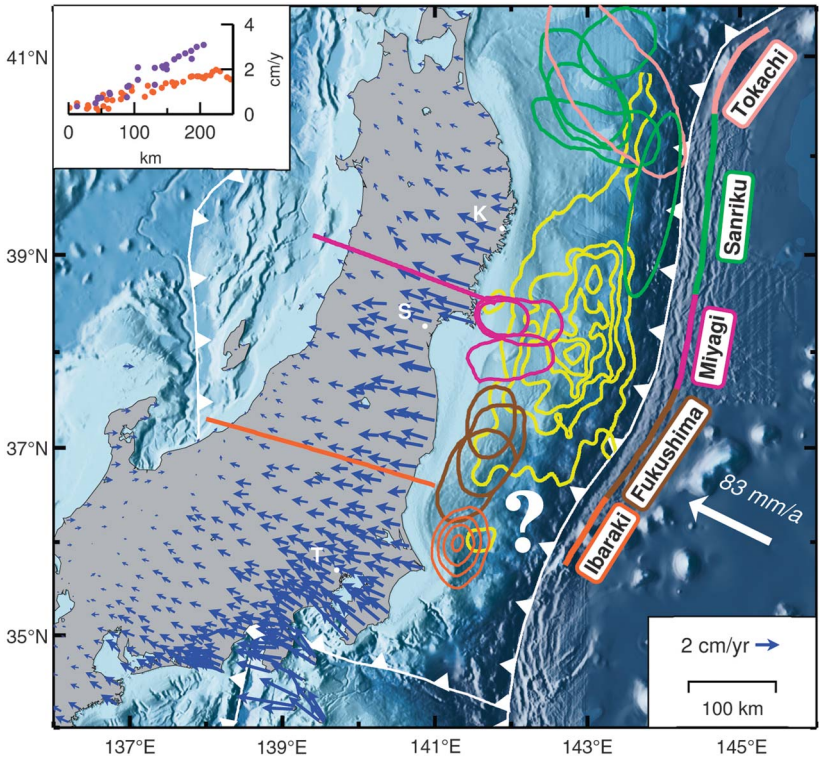

between 0.5 and 4 Hz from the 2010 Maule and 2011 Tohoku-Oki events (fig. S9). Although the value of peak slip inferred for the Tohoku-Oki earthquake was larger than for the Maule earthquake by a factor of about 2 to 3 and the area of appreciable slip for the Tohoku-Oki is approximately half that of the Maule earthquake, we find that the former produced much less HF radiation. We suggest that this difference is because the Maule earthquake rupture is on average much deeper than the Tohoku-Oki rupture (fig. S10). Thus, it may be that shallow ruptures generally produce large displacements with relatively weak HF excitation. Such an interpretation is also broadly consistent with the general observations that tsunami earthquakes rupture very slowly, with slip concentrated in the shallowest part of the megathrust (*25*).

Our inferred fault slip model suggests high static stress drop with large amounts of slip in a small region. An explanation for this behavior theorizes the existence of barriers that require much more stress accumulation than other regions before they rupture. Such barriers may pin the fault locally, limiting the amount of seismic slip occurring on neighboring areas that have lower thresholds for failure. When the strongest barrier finally ruptures, then surrounding areas can catch up. Subducted seamounts are the most obvious candidates for such barriers (*26*). Indeed, several seamounts are known to have subducted in this segment of the Japan Trench (*27*). The distribution of slip in the Tohoku-Oki earthquake suggests that small areas can have high effective yield stresses that serve to limit rupture propagation during some earthquakes but then eventually rupture with large slip during others.

The extent to which the 2011 earthquake was unexpected suggests that we should consider the potential for similar large events elsewhere on the Japan Trench megathrust. The secular interseismic velocity field for the Miyagi segment shows more than 3 cm/year of relative convergence across Honshu (Fig. 4). On average, faults in the interior and off the western coast of Honshu, are believed to account for between 1 and 2 cm/year (*28*)—leaving 1 to 2 cm/year associated with interseismic strain accumulation on the subduction interface. We adopt 1100 years as a representative time period because this corresponds to the last large event that is inferred to have occurred in this region (*4*). Thus, over this time period, we must still account for 11 to 22 m of relative motion across Honshu. Similarly, at about 8.5 cm/year of convergence, we must account for more than 90 m of fault slip on the megathrust.

Earthquake activity offshore of Miyagi (Fig. 1) has been suggested to be dominated by M7+ earthquakes recurring every 30 to 40 years (*2*). However, it has already been established that the historical events are not exact repeats of one another (*29*). Further, such M7+ events only produce 3 to 4 m of fault slip and 5 to 20 cm of surface displacement per event. In the 2011 mainshock, fault slip in the region of the historical M7+ events ranged from 5 to 25 m, which suggests that the concept of a characteristic subduction earthquake with approximately the same slip per event at a given location may be of limited use (*30*). That the 2011 event produced approximately 50 m of slip up-dip of the historical Miyagi M7+ events is roughly consistent with a 500- to 1000-year potential slip accumulation period. However, there is no basis on which to assume that the aforementioned interval of 1100 years is representative of the recurrence interval of great earthquakes in this segment—it could be shorter by a factor of 2 and still be consistent with the surface displacement budget and the peak slip inferred in this recent earthquake.

The only previously recorded large events offshore Fukushima and Ibaraki occurred as a sequence in 1938, which taken together correspond to about an M_w 8.1 event (*31*). At about 8.0 cm/year convergence, the 73 years since those earthquakes imply about 6 m of accumulated potential fault slip—surprisingly similar to the estimates of fault slip for this region during the 2011 event. However, this agreement is probably coincidental because there is no record of an equivalent set of earthquakes preceding the 1938 sequence. Similarly, the 2011 M_w 7.9 aftershock offshore of Ibaraki (Fig. 1) produced about 4 m of fault slip, implying a 50-year recurrence if these events are characteristic of this segment of the megathrust. There is no documentation of large (M8+) events prior to 1938 (*31*).

The 2 cm/year GPS-observed onshore convergence in this region (Fig. 4) implies that, in terms of the 1100-year budget, there is between 0 and 10 m of surface convergence that cannot be plausibly associated with faults farther to the west (*28*). The combination of the 2011 mainshock and the M7.9 aftershock only produced about 2 m of surface displacement.

There is no record of a large event up-dip of the 1938 Fukushima and Ibaraki sequence. Thus, the slip budget on the megathrust and the surface velocity data suggest that an earthquake similar to the 2011 event is possible offshore Ibaraki and Fukushima just south of the most recent event (Fig. 4). During such an event, the 1938 asperities and the M7.9 aftershock rupture area could experience much greater slip than has been documented for previous events, similar to what just occurred offshore Miyagi. However, if this region is in fact not strongly coupled, simple mechanical models (*32*) would predict high rates of postseismic afterslip—as is inferred to have occurred after several large recent earthquakes (*24*). Thus, it is essential to monitor this region to quantify the extent of any postseismic slip in order to further understand the long-term fault slip budget and associated seismic hazard.

References and Notes

1. C. DeMets, R. G. Gordon, D. F. Argus, *Geophys. J. Int.* **181**, 1 (2010).
2. "Seismic Activity in Japan—Regional Perspectives on the Characteristics of Destructive Earthquakes (Excerpt)" (Earthquake Research Committee, Headquarters for Earthquake Research Promotion, Prime Minister's Office, Tokyo, 1998).
3. C. Hashimoto, A. Noda, T. Sagiya, M. Matsu'ura, *Nat. Geosci.* **2**, 141 (2009).
4. K. Minoura, F. Imamura, D. Sugawara, Y. Kono, T. Iwashita, *J. Natural Disaster Sci.* **23**, 83 (2001).
5. See supporting material on *Science* Online.
6. S. E. Minson, M. Simons, J. L. Beck, paper presented at the AGU 2010 fall meeting, San Francisco, 13 to 17 December 2010, abstr. G12A-02.
7. Y. Tanioka, T. Seno, *Geophys. Res. Lett.* **28**, 3389 (2001).
8. A. Venkataraman, H. Kanamori, *J. Geophys. Res.* **109**, B05302 (2004).
9. C. Vigny *et al.*, *Science* **332**, 1417 (2011); 10.1126/science.1204132.
10. B. Delouis, J. M. Nocquet, M. Vallee, *Geophys. Res. Lett.* **37**, L17305 (2010).
11. C. Ji, D. J. Wald, D. V. Helmberger, *Bull. Seismol. Soc. Am.* **92**, 1208 (2002).
12. S. Ni, H. Kanamori, D. Helmberger, *Nature* **434**, 582 (2005).
13. M. Ishii, P. M. Shearer, H. Houston, J. E. Vidale, *Nature* **435**, 933 (2005).
14. R. Schmidt, *IEEE Trans. Antenn. Propag.* **34**, 276 (1986).
15. L. Borcea, G. Papanicolaou, C. Tsogka, *Inverse Probl.* **22**, 1405 (2006).
16. Y. Zeng, J. G. Anderson, G. Yu, *Geophys. Res. Lett.* **21**, 725 (1994).
17. T. H. Heaton, S. H. Hartzell, *Pure Appl. Geophys.* **129**, 131 (1989).
18. H. Nakahara, *Adv. Geophys.* **50**, 401 (2008).
19. M. Yamada, A. H. Olsen, T. H. Heaton, *Bull. Seismol. Soc. Am.* **99**, 3264 (2009).
20. A. A. Gusev, E. M. Guseva, G. F. Panza, *Pure Appl. Geophys.* **163**, 1305 (2006).
21. R. Madariaga, *Ann. Geophys.* **1**, 17 (1983).
22. Y. Ito, K. Obara, K. Shiomi, S. Sekine, H. Hirose, *Science* **315**, 503 (2007); 10.1126/science.1134454.
23. A. Sladen *et al.*, *J. Geophys. Res.* **115**, B02405 (2010).
24. Y. J. Hsu *et al.*, *Science* **312**, 1921 (2006).
25. J. Polet, H. Kanamori, *Geophys. J. Int.* **142**, 684 (2000).
26. M. Cloos, *Geology* **20**, 601 (1992).
27. K. Mochizuki, T. Yamada, M. Shinohara, Y. Yamanaka, T. Kanazawa, *Science* **321**, 1194 (2008).
28. J. P. Loveless, B. J. Meade, *J. Geophys. Res.* **115**, B02410 (2010).
29. H. Kanamori, M. Masatoshi, J. Mori, *Earth Planets Space* **58**, 1533 (2006).
30. S. Y. Schwartz, *J. Geophys. Res.* **104**, 23111 (1999).
31. K. Abe, *Tectonophysics* **41**, 269 (1977).
32. E. A. Hetland, M. Simons, *Geophys. J. Int.* **181**, 99 (2010).
33. Y. Tanioka, K. Sataka, *Geophys. Res. Lett.* **23**, 1549 (1996).
34. Z. Duputel *et al.*, http://eost.u-strasbg.fr/wphase/events/tohoku_oki_2011 (2011).

Acknowledgments: Supported in part by the Gordon and Betty Moore Foundation. M.S. and S.E.M. are supported by NSF grant CDI-0941374; J.P.A. and L.S.M. are supported by NSF grant EAR-1015704 and the Southern California Earthquake Center, which is funded by NSF Cooperative Agreement EAR-0106924 and USGS Cooperative Agreement 02HQAG0008. A portion of the research was carried out at the Jet Propulsion Laboratory (JPL), California Institute of Technology, under a contract with the National Aeronautics and Space Administration and funded through the internal Research and Technology Development program. We acknowledge the Geospatial Information Authority (GSI) of Japan for kindly providing all the GEONET RINEX data. Raw RINEX data are available directly from GSI. Processed GPS time series are provided through the ARIA project. We thank T. Ito for providing the interseismic velocity estimates used in Fig. 4. This paper is Caltech Tectonics Observatory contribution 165 and Caltech Seismological Laboratory contribution 10059.

Supporting Online Material

www.sciencemag.org/cgi/content/full/science.1206731/DC1
SOM Text
Figs. S1 to S12
Tables S1 and S2
References (*35*–*47*)

6 April 2011; accepted 11 May 2011
Published online 19 May 2011;
10.1126/science.1206731